

**Defect-enhanced selective ion transport in an ionic nanocomposite for efficient energy harvesting from moisture**

Dong Lv<sup>1</sup>, Shuang Zheng<sup>1\*</sup>, Chunyan Cao<sup>1</sup>, Kedi Li<sup>2</sup>, Liqing Ai<sup>1</sup>, Xin Li<sup>1</sup>, Zhengbao Yang<sup>3</sup>, Zhengtao Xu<sup>2</sup>, Xi Yao<sup>1\*</sup>

<sup>1</sup>Department of Biomedical Sciences, City University of Hong Kong, Hong Kong 999077, China

<sup>2</sup>Department of Chemistry, City University of Hong Kong, Hong Kong 999077, China

<sup>3</sup>Department of Mechanical Engineering, City University of Hong Kong, Hong Kong 999077, China

\*Correspondence and requests for materials should be addressed to S. Z. (Email: zhengshuang@iccas.ac.cn) or X. Y. (Email: xi.yao@cityu.edu.hk)

## Experimental Section

### *Materials.*

GO and [OMIM]Cl were purchased from J&K Scientific Ltd. Zn (NO<sub>3</sub>)<sub>2</sub>·6H<sub>2</sub>O (98.0 %), 2-Hmim (99.0 %) and methanol were purchased from Sigma-Aldrich. All chemicals were used as provided. Porous AAO membranes with a diameter of 25 mm were obtained from Shanghai Shangmu Tech.

### *Preparation of ZG and DZG nanosheets.*

20 ml of methanol solution with 0.94 g of Zn (NO<sub>3</sub>)<sub>2</sub>·6H<sub>2</sub>O, 20 ml of methanol solution with 2 g of 2-Hmim (molar ratio of 2-Hmim/Zn<sup>+</sup> was 8), and 10 ml of GO suspension in mixture solvent (deionized water: methanol of 1:1, v/v) with a concentration of 2 mg ml<sup>-1</sup> were mixed together by stirring for 5 h at room temperature. Then the ZG nanosheets were collected by centrifugation at 6000 rpm for 5 min and washed with methanol for several times. The thermal treatment of ZG nanosheets at various temperatures (250, 300, 325, 350 and 400°C, respectively) was carried out by placing samples in an alumina boat in a horizontal tube furnace with a heating rate of 5°C/min in air. Samples were calcinated for 1h after reaching the target temperatures. After cooling down to room temperature, the annealed samples were obtained for membrane preparation.

### *Device fabrication.*

The hybrid ZG and DZG nanosheets were re-dispersed in water to obtain a dispersion with a concentration of 0.2 mg ml<sup>-1</sup>. The dispersion was sonicated for 0.5 h. Then the dispersion was filtrated on the AAO template. After drying in dry oven at 60°C for overnight, the ZG and DZG membranes were obtained. 10 μL ILs ethanol solution with concentration of 0.8 g/ml was drop-casted on the MOFs-based membrane and blended evenly over a circular area with 10 mm in diameter. Then the fluid mixture film was dried in air for 1h to preliminarily remove ethanol. Afterwards, the membrane was dried in vacuum oven at 37°C for 5 h to allow for further leveling to obtain continuous ILs film. Finally, the membrane with Ag/AgCl mesh electrodes was placed

between two polymethyl methacrylate plates (4 cm × 4 cm × 1.2 cm bulk with a 10 mm cylindrical hole in center, Fig. S1c) to obtain the power generator.

#### *Characterizations.*

SEM images were obtained using a field emission scanning electron microscope (SEM, Philips XL30CP) at 7.0 kV. TEM image was collected by transmission electron microscope (Philips Tecnai 12). Optical image of DZG-325 membrane was recorded by a Nikon digital video camera. XRD test was performed by a Bruker D2 phaser diffractometer. FTIR spectra were taken by an FTIR spectrometer (PerkinElmer Spectrum 100). ATR-IR spectra were obtained on PerkinElmer Spectrum 100 equipped with an ATR accessory. TG analysis was examined on a TA Q600 differential thermal analyzer. The porosity and surface area analysis were conducted by a Quantachrome Autosorb iQ gas sorption analyzer.

#### *Water adsorption and transport test.*

The water adsorption of the ionic nanocomposite was determined by exposing the device to well controlled air atmosphere. The time-dependent weight changes of the device were recorded by an analytical balance (AX224, OHAUS Corporation, USA) which was sealed by a glass chamber (19\*22\*24 cm) to ensure a constant humidity. Before test, the [OMIM]Cl was placed in dry oven at 80 °C for 24 h to completely remove water. The humidity of air in the balance was controlled by adding water or calcium chloride (AR, Aladdin). The mass of the device was recorded at certain time intervals. The water content in the device was calculated by the following the equation:  $WC = (m_1 - m_0) / m_0 \times 100\%$ , where  $m_0$  and  $m_1$  are the weight of device before and after water absorption. The water transport rate after achieving moisture absorption/desorption equilibrium was also studied by recording the time-dependent mass loss of the system.

#### *Electrical measurements.*

Power generation performance of the device was investigated by using a homemade

instrument (Fig. S1c). The ionic nanocomposite was mounted between two self-made compartments. Self-made Ag/AgCl mesh were used as electrodes for determining  $V_{oc}$  and  $I_{sc}$  (Figure S12, Supporting Information). The  $V_{oc}$  and  $I_{sc}$  were recorded by a DMM6500 digital multimeter (Keithley Instruments). The I-V curve was collected by a Picoammeter (Keithley 6487). Power density was assessed by measuring the voltage and current of the circuit incorporating with a series of external loads. The effective testing area for power density is 1 mm<sup>2</sup>. The skin-induced power generation was reviewed and approved by the JCC College Human Ethics Sub-committee of City University of Hong Kong (jcc2122ay003).

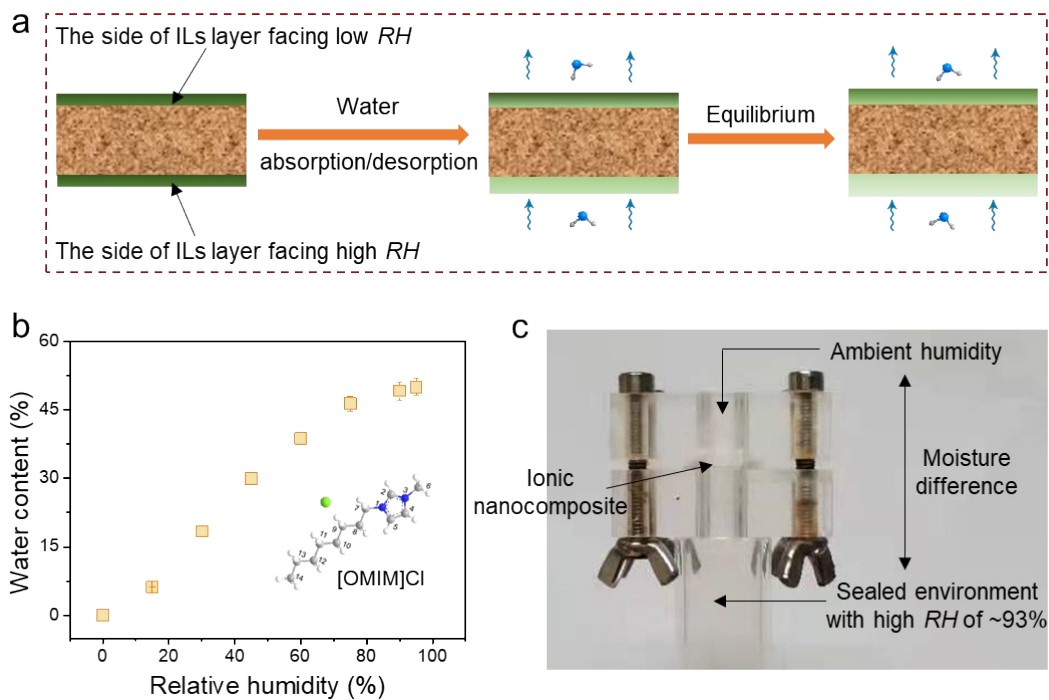


**Figure S1. Fabrication of moisture-enabled power generator. a,** The process of water absorption/desorption within the ionic nanocomposite. **b,** Water uptake of [OMIM]Cl in different *RH* at room temperature. **c,** Experimental set-up for moisture-sustained energy harvesting with a sealed high *RH* environment.

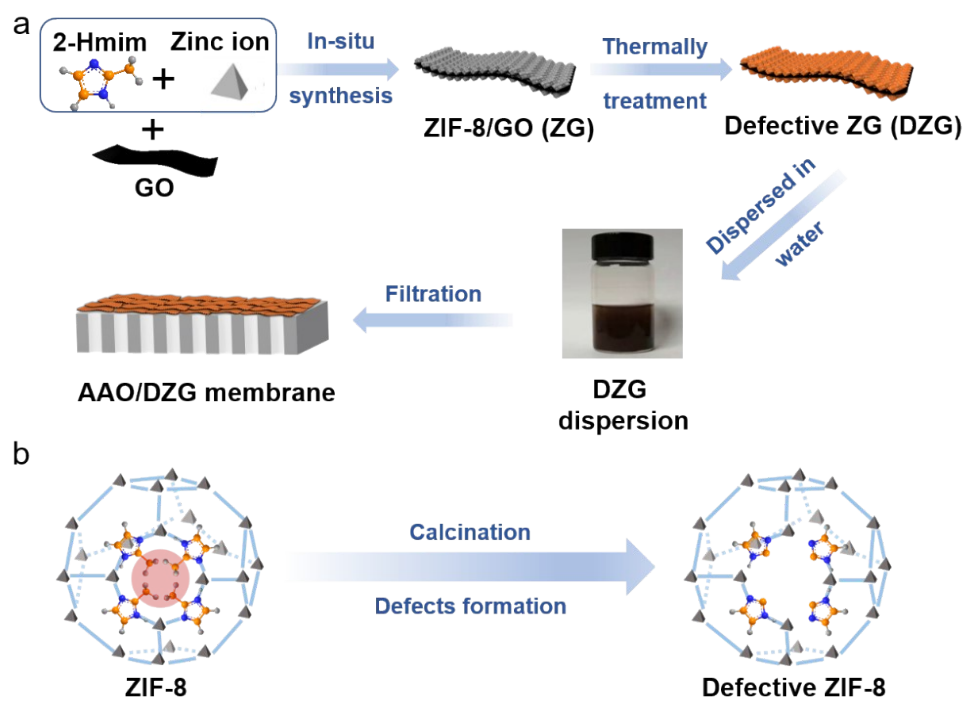


**Figure S2. Schematic illustration of preparation process of defective ZIF-8/GO membrane. a,** Fabrication process of ZG and DZG membrane. **b.** Introduction of vacancies in ZIF-8 nanoparticles by calcination.

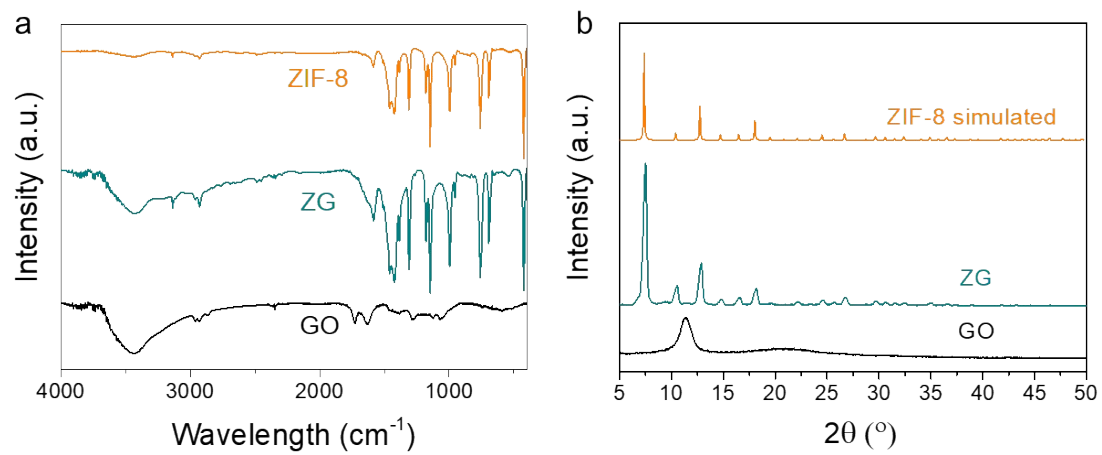


**Figure S3.** FTIR (a) and XRD (b) of ZIF-8, ZG and GO, indicating the successful growth of ZIF-8 on GO nanosheets.

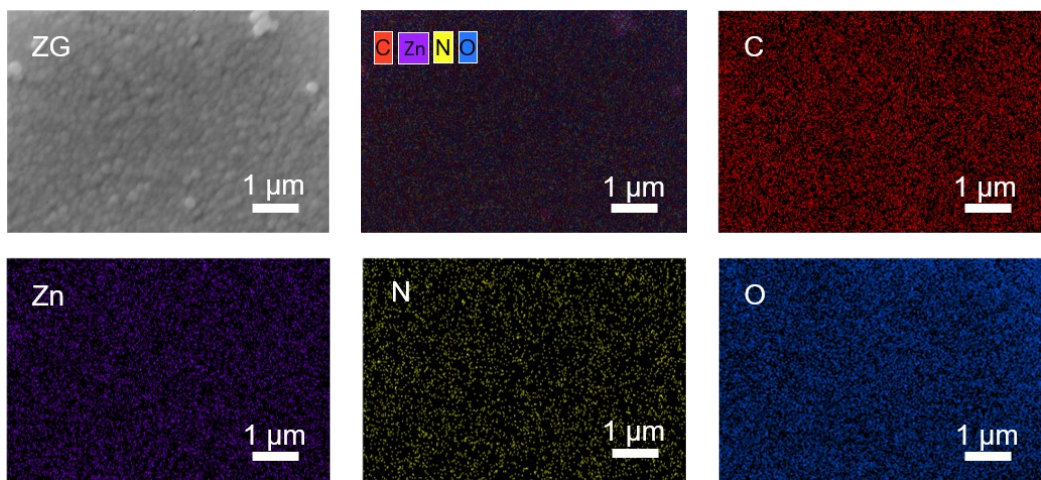


**Figure S4.** SEM images of ZG nanosheets and its corresponding EDX element mapping (C, Zn, N and O).

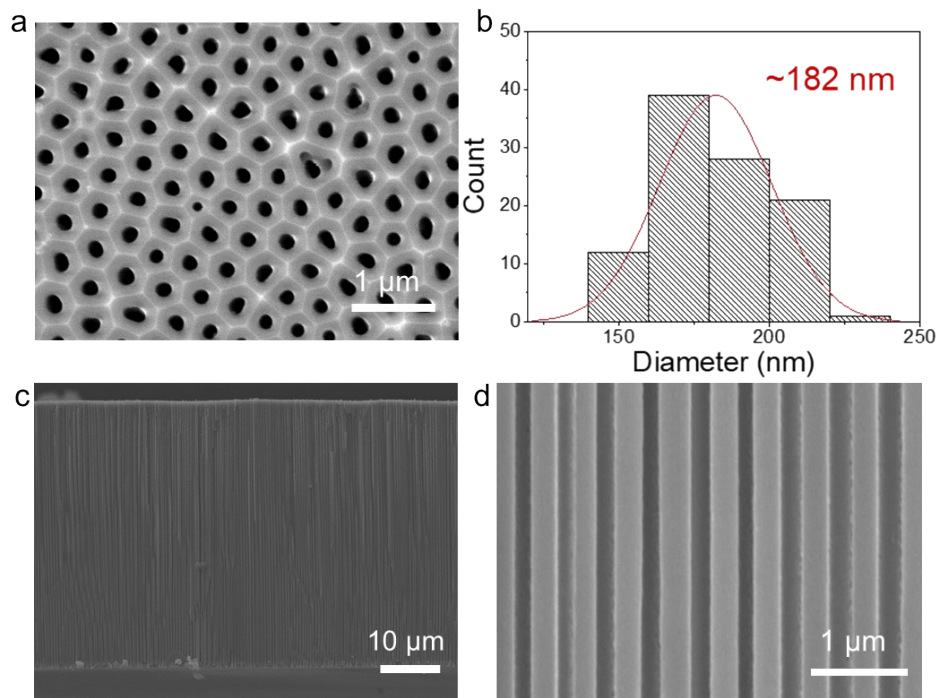


**Figure S5. Characterization of AAO membrane.** **a**, Surface SEM image of AAO membrane. **b**, Data statistics of the pore diameter of AAO membrane in **a**. Regular **(c)** and high resolution **(d)** cross-sectional SEM images of AAO membrane.

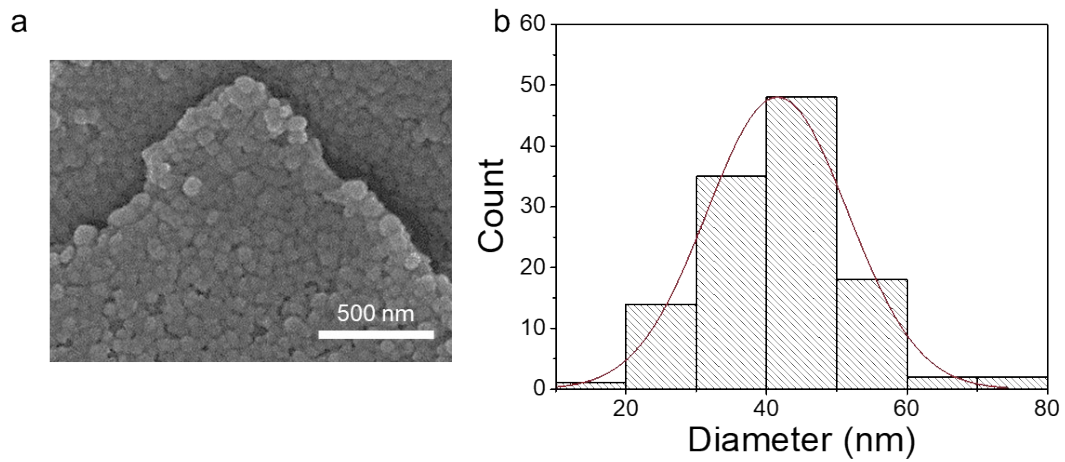


**Figure S6. a**, SEM image of DZG-325 nanosheets. **b**, Data statistics of the size of ZIF-8 grown on GO nanosheets.

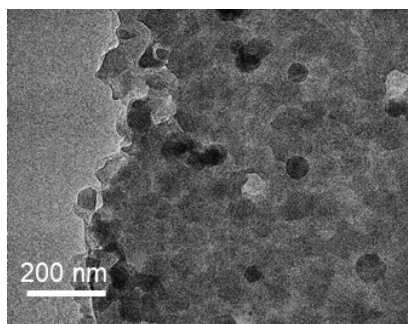


**Figure S7.** The TEM image of DZG-325.

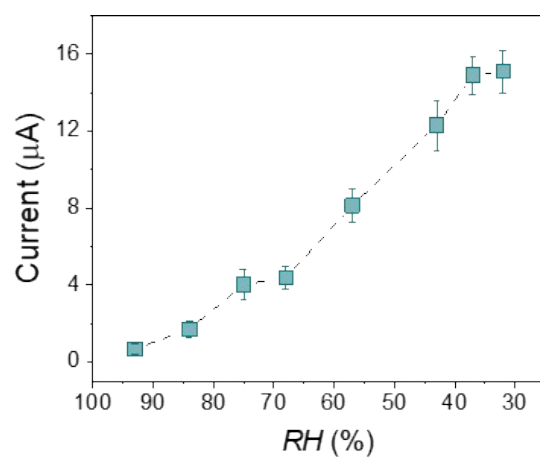


**Figure S8.**  $I_{sc}$  performance of DZG-325 generator as a function of environmental  $RH$ .

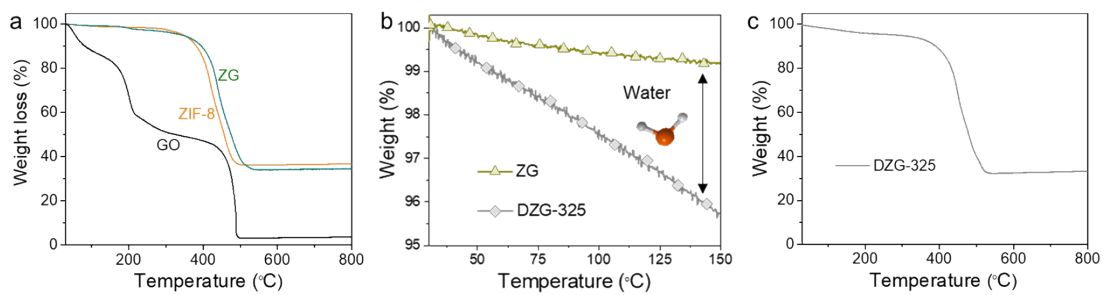


**Figure S9. a,** TG analysis of ZIF-8, ZG and GO. **b,** TG analysis of ZG and DZG-325 nanosheets, indicating the higher water retention ability of DZG-325 sample. **c,** Full range TGA curve of DZG-325.

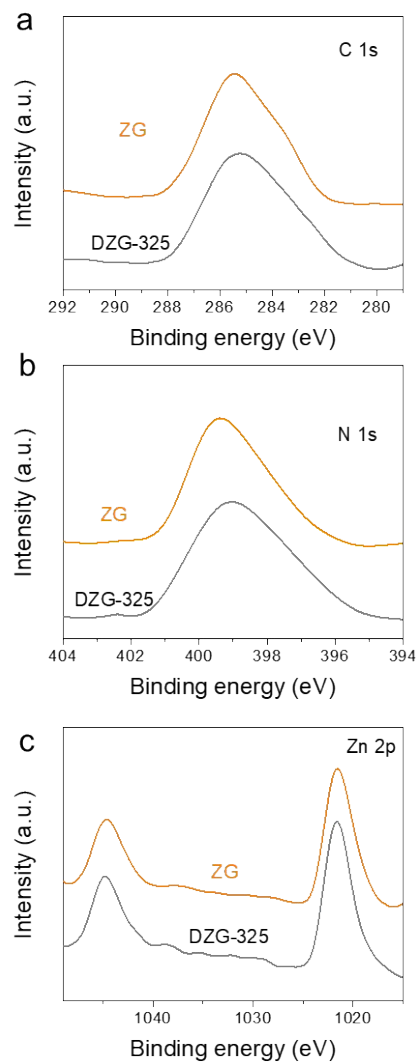


**Figure S10.** XPS C 1s (a), N 1s (b) and Zn 2p (c) core level spectra of ZG and DZG-325.

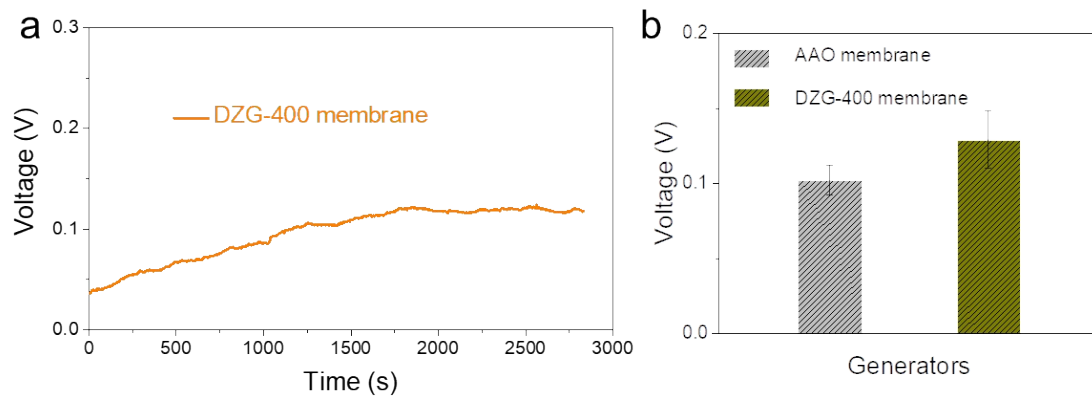


**Figure S11. Power generation performance of power generator using DZG-400 membrane. a,**  $V_{oc}$  output of DZG-400 generator as a function of time. **b,** Comparison of  $V_{oc}$  obtained by generators using AAO membrane and DZG-400 membrane.

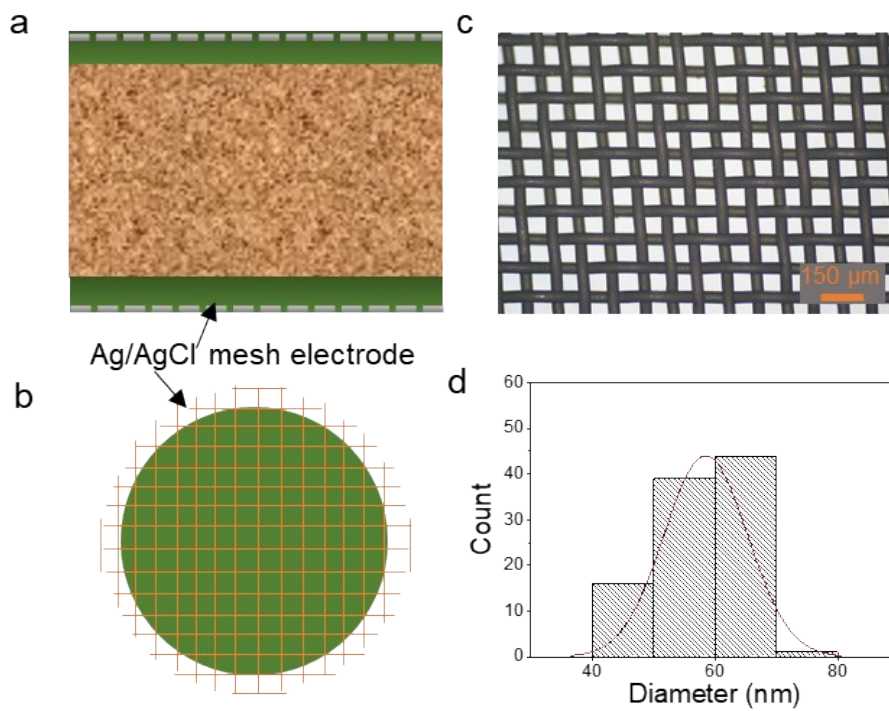


**Figure S12.** Schematic illustration of the sectional (a) and frontal (b) structure of Ag/AgCl mesh electrode. c, Optical image of meshed Ag/AgCl wires. d, Data statistics of window size of Ag/AgCl mesh in c.

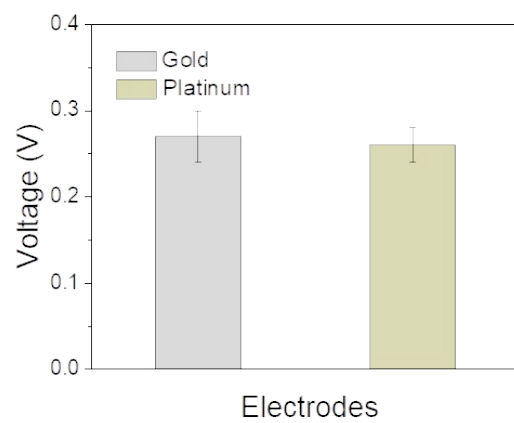


**Figure S13.** Energy output of power generator using different inert electrodes.

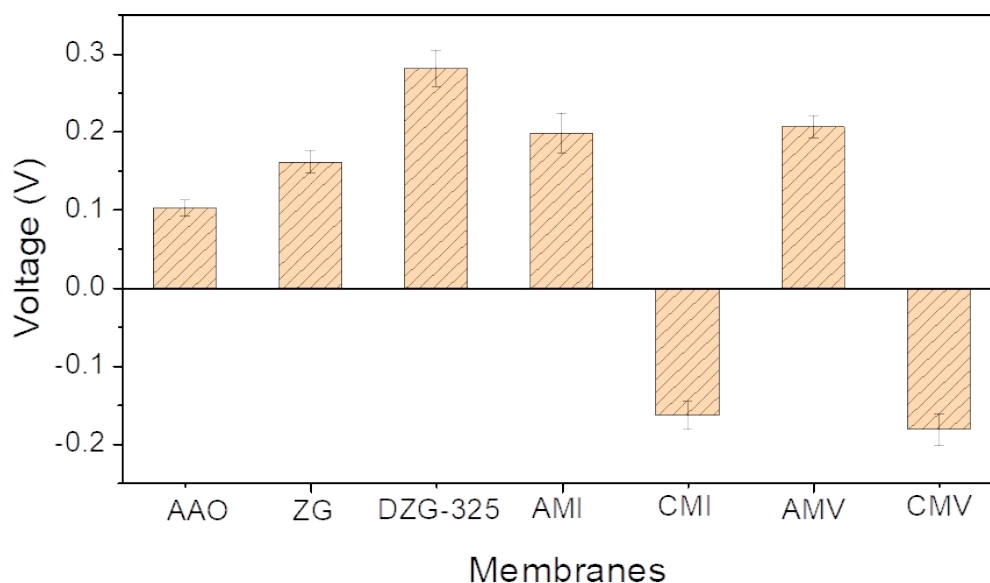


**Figure S14.** Comparison of electricity output performance by power generators using AAO, ZG, DZG-325 and commercial membranes.

**AMI** (AMI-7001, Membranes International Inc.) is strong base anion exchange membrane, which has polymer structure of gel polystyrene cross linked with divinylbenzene and functional group of quaternary ammonium. **CMI** (CMI-7000, Membranes International Inc.) is strong acid cation exchange membrane, which has polymer structure of gel polystyrene cross linked with divinylbenzene and functional group of sulphonic acid. **AMV** (AGC Engineering Co.) is homogenous anion exchange membrane with fixed strong basic ionic group of quaternary ammonium. **CMV** (AGC Engineering Co.) is cation exchange membrane made of crosslinked polystyrene with fixed ionic group of sulphonic acid.

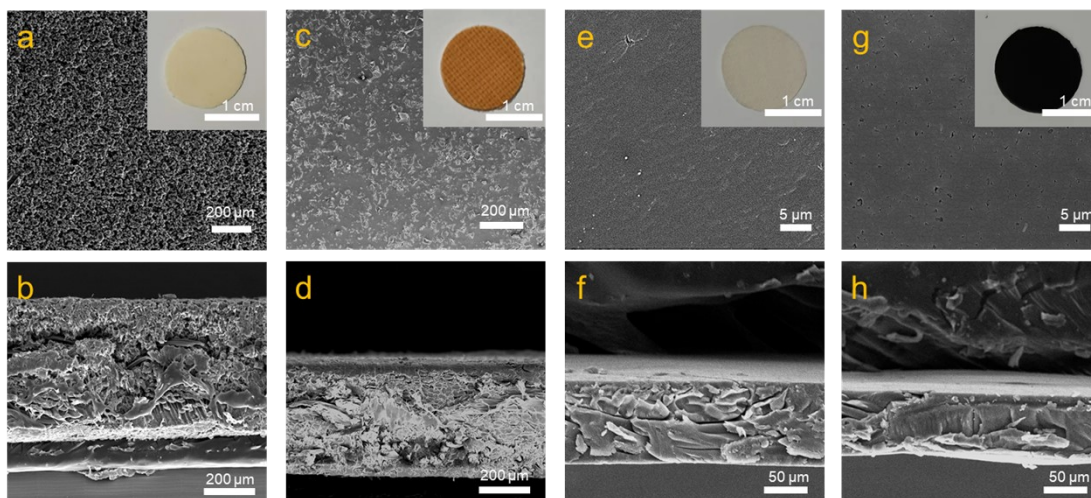


**Figure S15. Surface and side-view SEM images of commercial membranes. (a and b)** AMI, **(c and d)** CMI, **(e and f)** AMV and **(g and h)** CMV. Insets are the optical images of the commercial membranes at dry form. The commercial membranes are cut into disc with a diameter of 15 mm.

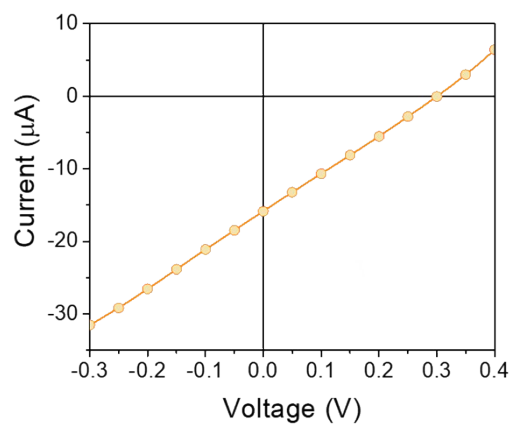


**Figure S16.** The I-V curve of DZG-325 generator.

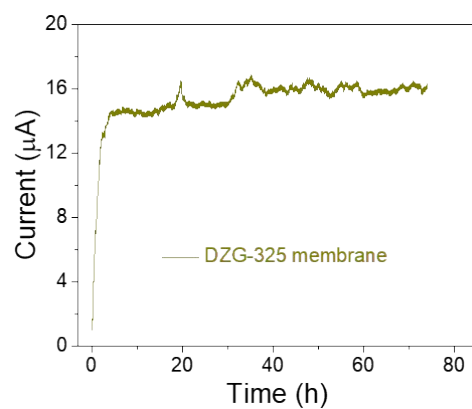


**Figure S17.** Long-term monitoring of  $I_{sc}$  output for power generator using DZG-325 membranes.

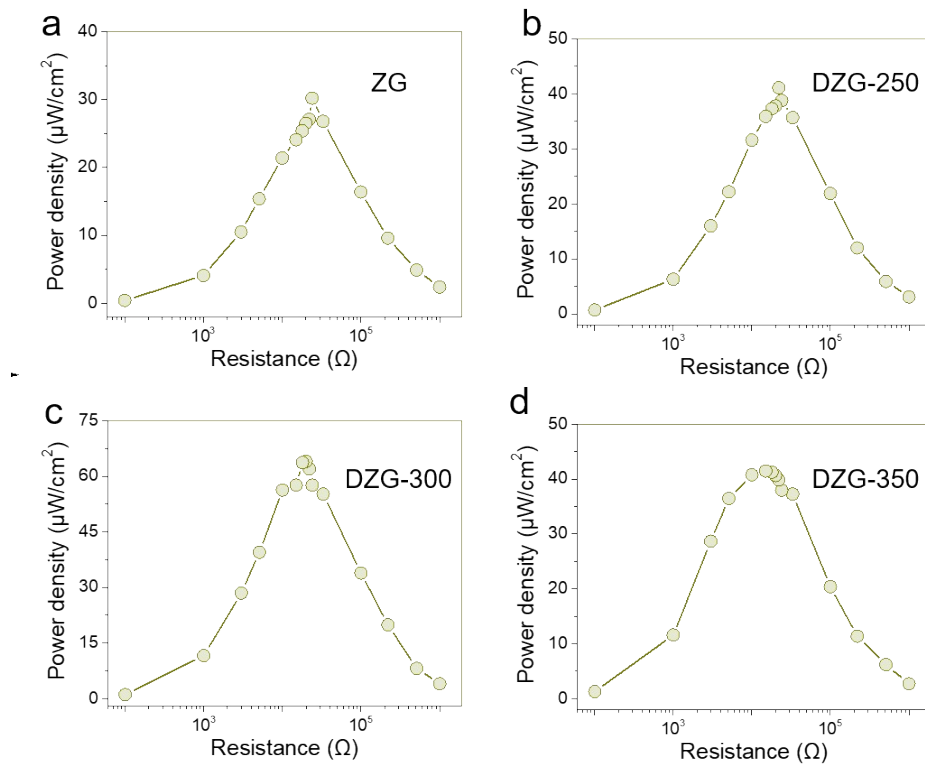


**Figure S18. Power density dependencies on samples with various calcination temperature. (a) ZG, (b) DZG-250, (c) DZG-300, and (d) DZG-350.**

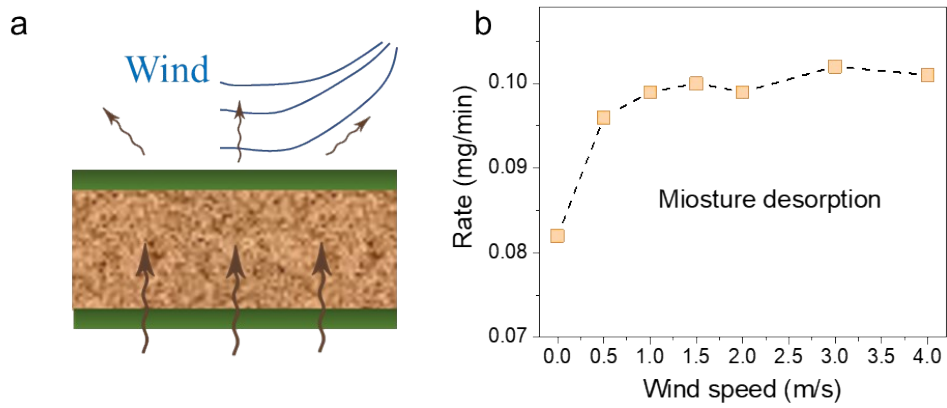


**Figure S19. Wind facilitated electricity output.** **a**, Schematic illustration of wind promoted moisture evaporation from surface of the power generator. **b**, Dependence of the measured moisture desorption rate on the wind blowing speed (0-4 m/s).

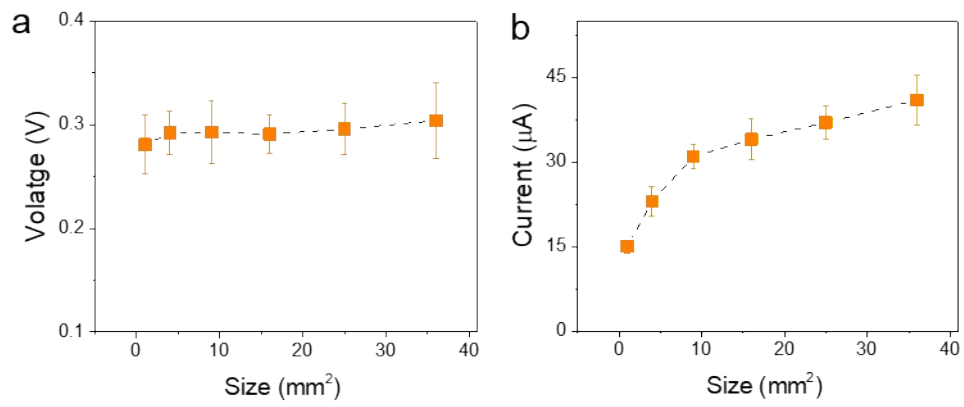


**Figure S20.** (a)  $V_{oc}$  and (b)  $I_{sc}$  as function of membrane size for DZG-325 generator.

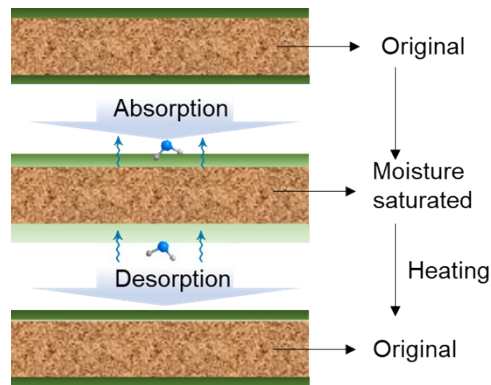


**Figure S21. Heat-assisted reactivation of the moisture-saturated generator.**

Schematic illustration of spontaneous water adsorption and heating-assisted water desorption within ILs-infused film.

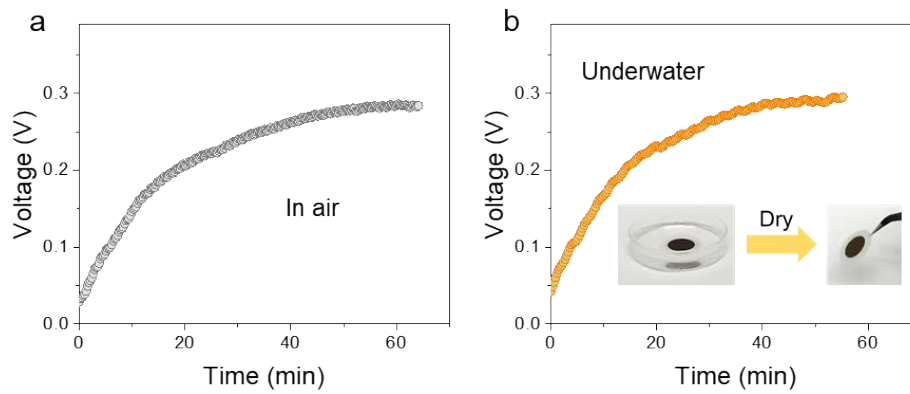


**Figure S22.  $V_{oc}$  output of generators using stored DZG-325 membranes, (a) in air for more than 3 month and (b) underwater for one week.**

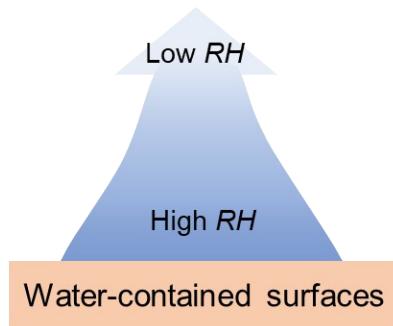


**Figure S23.** Schematic illustration of moisture difference induced by vapor evaporation from water-contained surfaces such as animal skin, soil, vehicles and buildings, which can be served as moisture sources.

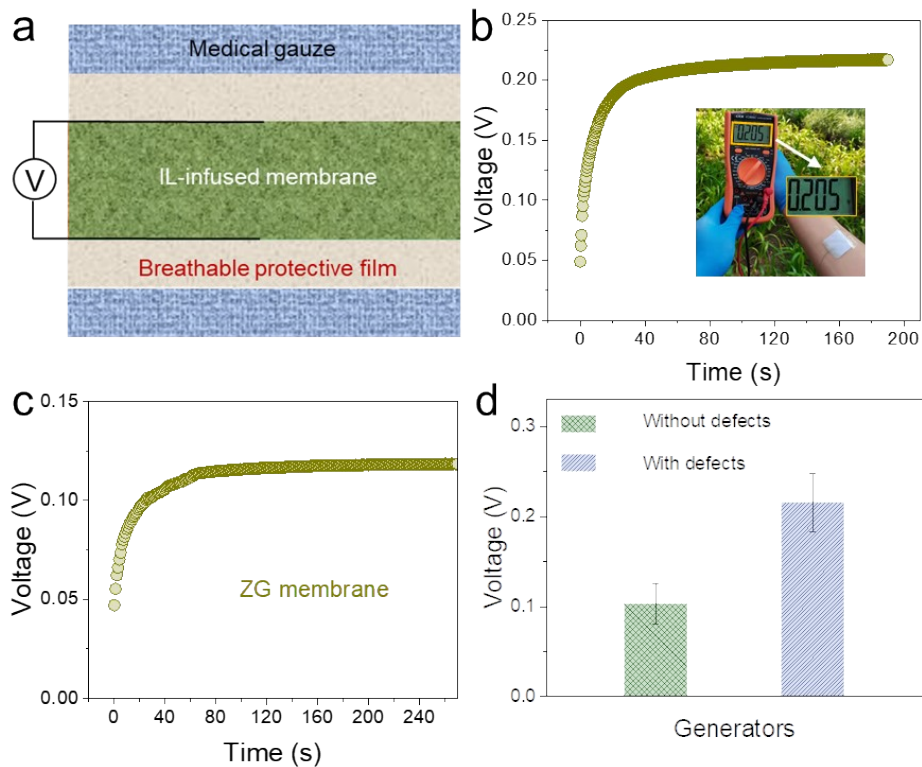


**Figure S24.** Power generation of DZG-325 generator using human skin as humidity source. **a**, Schematic illustration of the structure of power generator for human skin-induced power generation.  $V_{oc}$  curves obtained by DZG-325 generator (**b**) and ZG generator (**c**) using human skin as humidity source. **d**, Impact of defects on electricity output when human skin was used as humidity source.

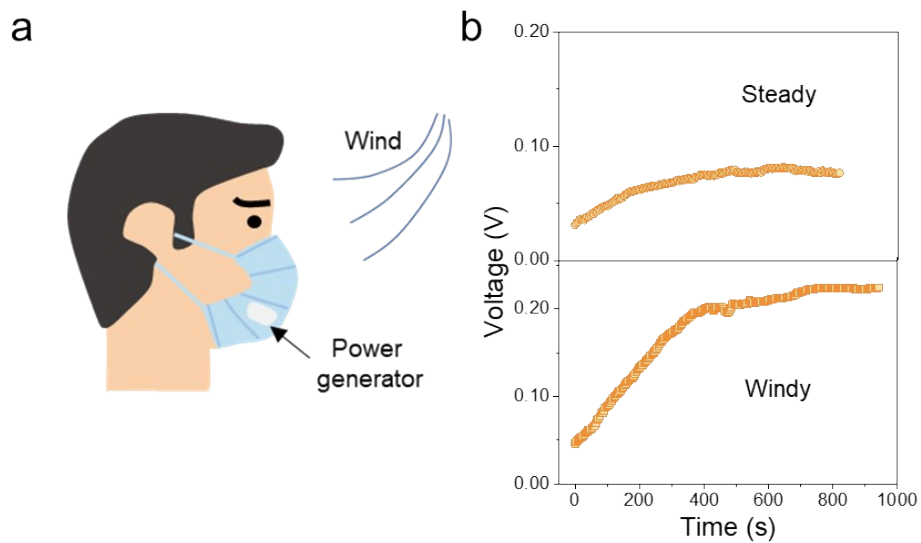


**Figure S25. a,** Schematic illustration of the impact of small wind to the humidity difference across the generator. **b,**  $V_{oc}$  output by DZG-325 generator using mask surface as humidity source at steady or windy states.

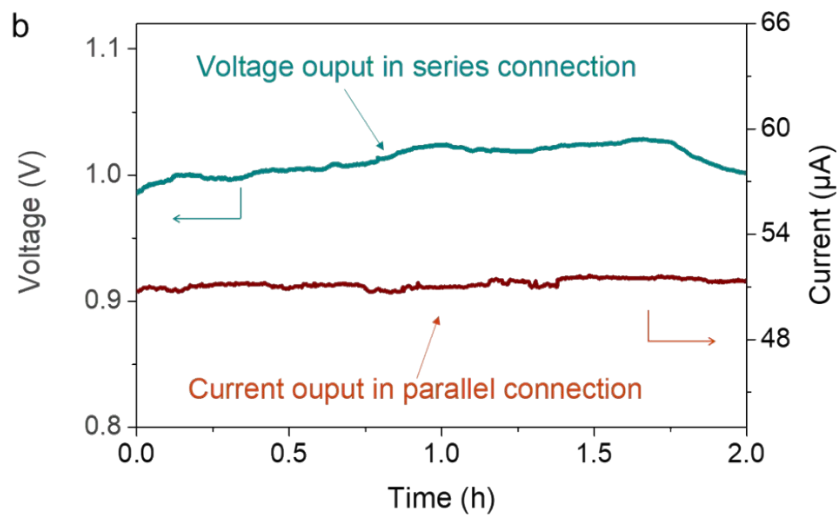
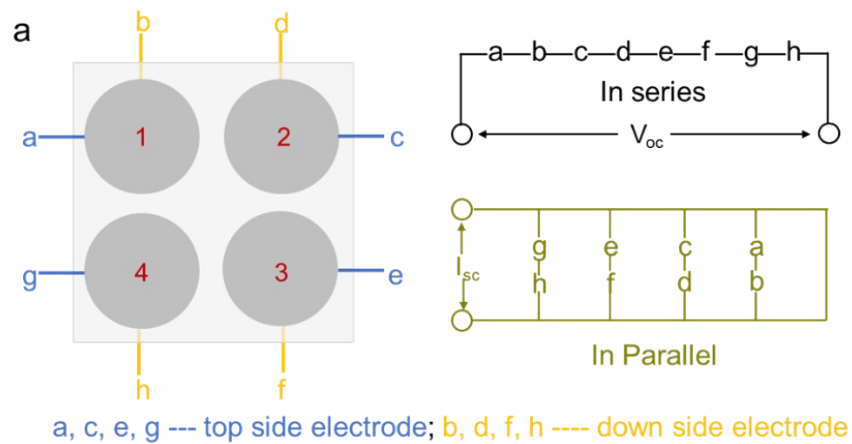


**Figure S26. Integration of power generators. a,** Electrode connection of generators in series and parallel connections. **b,**  $V_{oc}$  output of four generators in series connection and  $I_{sc}$  output of four generators in parallel connection.

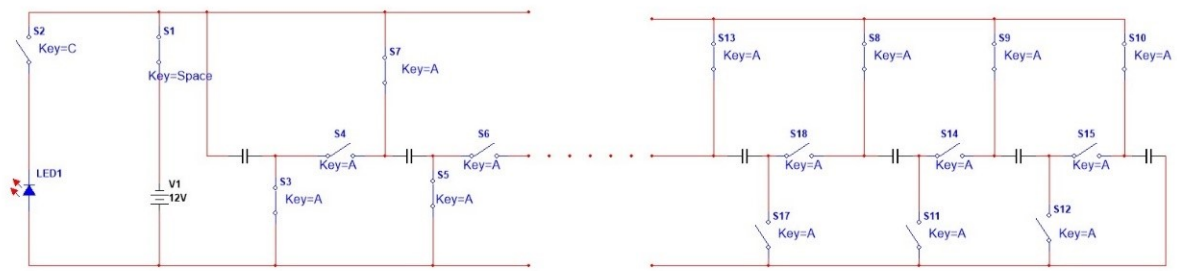


**Figure S27.** Charging and discharging circuit for collecting energy produced by DZG-325 generator.  $S_x$  represent switches.

**Table S1.** Chemical compositions (atomic%) of ZIF-8 and calcinated ZIF-8 (325°C) samples from EDX measurement.

	ZIF-8	Calcinated ZIF-8
C	62.04	55.02
N	30.62	36.27
Zn	7.34	8.71

**Table S2.** Specific surface area (SSA) and micropore volume ( $V_{\text{micro}}$ ) of samples.

	ZG	DZG-250	DZG-300	DZG-325	DZG-350	DZG-400
SSA ( $\text{m}^2 \text{g}^{-1}$ )	1690	1556	1248	1191	923	251
$V_{\text{micro}}$ ( $\text{cm}^3 \text{g}^{-1}$ )	0.641	0.618	0.606	0.473	0.438	0.263

**Table S3.** Performance comparison of humidity-driven generators with continuous electricity output.

<b>Materials</b>	<b>Humidity source</b>	<b>Current density (<math>\mu\text{A}/\text{cm}^2</math>)</b>	<b>Power density (<math>\mu\text{W}/\text{cm}^2</math>)</b>	<b>Ref.</b>
Graphene oxide	Human breathing	0.01	0.42	1
Conductive polymer	Manmade wet and dry nitrogen	2.3	0.69	2
Graphene oxide	Manmade wet and dry nitrogen	0.0045	2.02	3
Protein nanowire	Ambient moisture	17	5	4
Polyelectrolyte	Ambient moisture	0.06	5.52	5
Graphene oxide	Ambient moisture	1	0.07	6
Biological nanofibrils	Ambient moisture	0.025	0.0063	7
Cellulose acetate	Ambient moisture	0.08	0.0084	8
P(MEDSAH-co-AA)	Ultrasonic humidifier	1.5	0.15	9
Electrospun nanofiber	Ambient moisture	1.35	1.48	10
Carbon nanoparticle	Water stream	0.83	0.075	11
Graphene oxide monolith	Ambient moisture	6.2	0.07	12
Graphene oxide and reduced graphene oxide	Human breathing	4.5	0.42	13
Graphitic carbon	Water vapor and dry nitrogen	0.4	0.093	14
Electrospun nanofiber fabric	Ambient moisture	0.03	0.0062	15
G.S. nanowires	Ambient moisture	7.5	2.5	16

Note: (1) P(MEDSAH-co-AA refers to poly([2-(methacryloyloxy)ethyl] dimethyl-(3-sulfopropyl) ammonium hydroxide-co-acrylic acid). (2) G.S. nanowires refers to *Geobacter sulfurreducens* nanowires.

### Citing reference in Table S1

- [1] Zhao, F., Cheng, H.H., Zhang, Z.P., Jiang, L. & Qu, L.T. Direct power generation from a graphene oxide film under moisture. *Adv. Mater.* **27**, 4351-4357 (2015).
- [2] Xue, J.L., Zhao, F., Hu, C.G., Zhao, Y., Luo, H.X., Dai, L.M. & Qu, L.T. Vapor-activated power generation on conductive polymer. *Adv. Funct. Mater.* **26**, 8784-8792 (2016).
- [3] Cheng, H.H., Huang, Y.X., Zhao, F., Yang, C., Zhang, P.P., Jiang, L., Shi, G.Q. & Qu, L.T. Spontaneous power source in ambient air of a well-directionally reduced graphene oxide bulk. *Energy Environ. Sci.* **11**, 2839-2845 (2018).
- [4] Liu, X.M., Gao, H.Y., Ward, J.E., Liu, X.R., Yin, B., Fu, T.D., Chen, J.H., Lovley, D.R. & Yao, J. Power generation from ambient humidity using protein nanowires. *Nature* **578**, 550-554 (2020).
- [5] Wang, H.Y., Sun, Y.L., He, T.C., Huang, Y.X., Cheng, H.H., Li, C., Xie, D., Yang, P.F., Zhang, Y.F. & Qu, L.T. Bilayer of polyelectrolyte films for spontaneous power generation in air up to an integrated 1,000 V output. *Nat. Nanotechnol.* **16**, 811-819 (2021).
- [6] Huang, Y.X., Cheng, H.H., Yang, C., Yao, H.Z., Li, C. & Qu, L.T. All-region-applicable, continuous power supply of graphene oxide composite. *Energy Environ. Sci.* **12**, 1848-1856 (2019).
- [7] Li, M.J., Zong, L., Yang, W.Q., Li, X.K., You, J., Wu, X.C., Li, Z.H. & Li, C.X. Biological nanofibrous generator for electricity harvest from moist air flow. *Adv. Funct. Mater.*, **29**, 1901798 (2019).
- [8] Lyu, Q.L., Peng, B.L., Xie, Z.J., Du, S., Zhang, L.B. & Zhu, J.T. Moist-Induced Electricity Generation by Electrospun Cellulose Acetate Membranes with Optimized Porous Structures. *ACS Appl. Mater. Interfaces* **12**, 57373-57381 (2020).
- [9] Long, Y., He, P.S., Shao, Z.C., Li, Z.Y., Kim, H., Yao, A.M.Z., Peng, Y.D., Xu, R.X., Ahnl, C.H., Lee, S.W., Zhong, J.W. & Lin, L.W. Moisture-induced autonomous surface potential oscillations for energy harvesting. *Nat Commun* **12**, 5287 (2021).
- [10] Sun, Z.Y., Feng, L.L., Wen, X., Wang, L.M., Qin, X.H. & Yu, J.Y. Nanofiber fabric based ion-gradient-enhanced moist-electric generator with a sustained voltage output of 1.1 volts. *Mater. Horizons* **8**, 2023 (2021).
- [11] Bae, J., Yun, T.G., Suh, B.L., Kim, J. & Kim, I.D. Self-operating transpiration-driven electrokinetic power generator with an artificial hydrological cycle. *Energy Environ. Sci.* **13**, 527-534 (2020).
- [12] Liu, J., Qi, Y., Liu, D.P., Dong, D.P., Liu, D.D. & Li, Z.H. Moisture-enabled electricity generation from gradient polyoxometalates-modified sponge-like graphene oxide monolith. *J. Mater. Sci.* **54**, 4831-4841 (2019).
- [13] Yang, C., Huang, Y.X., Cheng, H.H., Jiang, L. & Qu, L.T. Rollable, stretchable, and

- reconfigurable graphene hygroelectric generators. *Adv. Mater.* **31**, 1805705 (2019).
- [14] Lee, S., Jang, H., Lee, H., Yoon, D. & Jeon, S. Direct fabrication of a moisture-driven power generator by laser-induced graphitization with a gradual defocusing method. *ACS Appl. Mater. Interfaces* **11**, 26970-26975 (2019).
- [15] Sun, Z.Y., Feng, L.L., Xiong, C.D., He, X.Y., Wang, L.M., Qin, X.H. & Yu, J.Y. Electrospun nanofiber fabric: an efficient, breathable and wearable moist-electric generator. *J. Mater. Chem. A* **9**, 7085-7093 (2021).
- [16] Ren, G.P., Wang, Z., Zhang, B.T., Liu, X., Ye, J., Hu, Q.C. & Zhou, S.G. A facile and sustainable hygroelectric generator using whole-cell *Geobacter sulfurreducens*. *Nano Energy* **89**, 106361 (2021).